Kinetic framework of spindle assembly checkpoint signaling

Amalie E. Dick[1,2,3] and Daniel W. Gerlich[1,2,3]*

[1]Institute of Molecular Biotechnology of the Austrian Academy of Sciences (IMBA), 1030 Vienna, Austria

[2]Institute of Biochemistry, ETH Zurich, 8093 Zurich, Switzerland

[3]Marine Biological Laboratory, Woods Hole, MA 02543, USA

*Address correspondence to DWG. E-mail: daniel.gerlich@imba.oeaw.ac.at

The mitotic spindle assembly checkpoint (SAC) delays anaphase onset until all chromosomes have attached to both spindle poles[1, 2]. Here, we investigated SAC signaling kinetics in response to acute detachment of individual chromosomes using laser microsurgery. Most detached chromosomes delayed anaphase until they had realigned to the metaphase plate. A substantial fraction of cells, however, entered anaphase in the presence of unaligned chromosomes. We identify two mechanisms by which cells can bypass the SAC: First, single unattached chromosomes inhibit the anaphase promoting complex/cyclosome (APC/C) less efficiently than a full complement of unattached chromosomes. Second, because of the relatively slow kinetics of re-imposing APC/C inhibition during metaphase, cells were unresponsive to chromosome detachment up to several minutes before anaphase onset. Our study defines when cells irreversibly commit to enter anaphase and shows that the SAC signal strength correlates with the number of unattached chromosomes. Detailed knowledge about SAC signaling kinetics is important for understanding the emergence of aneuploidy and the response of cancer cells to chemotherapeutics targeting the mitotic spindle.

Spindle assembly is an error prone process, which can involve multiple rounds of microtubule attachment and detachment on individual kinetochores[3, 4]. Incorrectly attached chromosomes, for example when both sister kinetochores bind to the same spindle pole, are detected by an error correction machinery, which depolymerizes microtubules on kinetochores if they are under low mechanical tension (reviewed in [5]). This enables chromosomes to eventually attach their sister kinetochores to microtubules originating from opposing spindle poles.

Due to the stochastic nature of spindle assembly, anaphase must be robustly delayed when individual chromosomes fail to attach properly. Indeed, a single unattached kinetochore can delay anaphase onset for up to several hours in PtK_1 cells[6]. Yet, even when all kinetochores are unattached by drug-induced depolymerization of microtubules, cyclin B continues to be degraded by low residual APC/C activity, which leads to mitotic exit in presence of an active SAC (mitotic slippage)[7-9]. Mitotic slippage occurs at different rates in a variety of cancer and non-cancer cells and it has been proposed as a mechanism by which cancer cells may develop resistance against therapeutics that target the mitotic spindle[8-12]. Hence, it is important to better understand the signaling kinetics underlying SAC-mediated APC/C inhibition.

Unattached kinetochores recruit the SAC protein Mad2 to promote assembly of cytoplasmic mitotic checkpoint complex, composed of Mad2, Bub3, BubR1, and Cdc20 (reviewed in [1, 2]). The mitotic checkpoint complex suppresses anaphase entry by inhibiting APC/C binding to

metaphase substrates like cyclin B and securin. Current models posit that continuous turnover of mitotic checkpoint complex on APC/C by Cdc20 autoubiquitylation enables rapid response of the SAC to the chromosome attachment status, as it liberates APC/C to bind free Cdc20 once the SAC has been satisfied[13-18].

Little is known about the kinetics and efficiency by which the SAC and the APC/C respond to individual chromosome attachment/detachment events. We therefore set out to measure SAC signaling in live cells, using quantitative microscopy and biophysical spindle perturbations.

To study the kinetics by which cells mount a SAC signal, we developed a laser microsurgery procedure for acute detachment of kinetochore fibers from individual chromosomes. HeLa cells stably expressing the chromatin marker histone 2B (H2B) tagged with mCherry, and the spindle marker mEGFP-α-tubulin were cut by a high-energy pulsed laser on microtubules at the edge of the mitotic spindle (Fig. 1a). This released one (n = 20 cells) or few (n = 15 cells) chromosomes from the metaphase plate. The displaced chromosomes always moved towards the spindle pole opposing the site of the cut, presumably driven by pulling forces generated at the sister kinetochore that remained connected to the spindle.

We next investigated how laser microsurgery affected the kinetochore-microtubule interface. To determine the SAC signaling state on laser-detached chromosomes we used HeLa cells stably expressing mouse Mad2-EGFP from its endogenous promoter and H2B-mCherry. Mouse Mad2-EGFP is functional in HeLa cells, as it effectively restored a nocodazole-induced arrest after RNAi-mediated depletion of the endogenous human Mad2 (Supplementary Fig. S1a-c). Following laser microsurgery and live-cell imaging (Fig. 1b, Supplementary Fig. S1d), we fixed cells for correlative microtubule immunofluorescence staining (Fig. 1c, Supplementary Fig. S1e). 27 chromosomes were displaced from metaphase spindles in 18 cells, and all displaced chromosomes had accumulated Mad2-EGFP at the time of fixation (2:20 to 6:00 min:s after laser microsurgery), either on a pair of dots (18 chromosomes; Fig. 1c, d) or on a single dot (9 chromosomes; Fig. 1e, Supplementary Fig. S1d, e). This indicates that laser microsurgery efficiently induces SAC signaling on displaced chromosomes.

Previous work indicates that monotelically attached kinetochores can accumulate low levels of Mad2[19]. Most laser-displaced chromosomes accumulated Mad2-EGFP to similarly high levels on both sister kinetochores (Supplementary Fig. S1f), suggesting that laser microsurgery had completely detached the respective chromosomes. This is unlikely to be

caused by kinetochore damage given the proficiency in Mad2-EGFP accumulation. Rather, we suspect that a drop in mechanical tension between sister kinetochores may have stimulated microtubule disassembly on both sister kinetochores by the error correction machinery[5]. Monotelic chromosomes induced by laser microsurgery thus appear to be less stably attached to microtubules compared to previously observed spontaneously occurring monotelic chromosome attachments[6]. A possible explanation for this may be the dissociation of Polo like kinase 1 (Plk1) from kinetochores when chromosomes have aligned on the metaphase plate[20, 21]. This changes the microtubule-kinetochore interface from a state that favors initial stable interactions to a more dynamic attachment state that enables efficient attachment error correction during metaphase[21].

Following laser microsurgery, most chromosomes moved along the edge of the spindle. The high microtubule density at these regions precluded a comprehensive analysis of chromosome interactions with microtubules by immunofluorescence microscopy and we therefore focused our analysis on Mad2-positive kinetochores. 31 out of 45 Mad-EGFP dots on laser-displaced chromosomes localized just at the edge of the spindle (Fig. 1c, d), consistent with previously observed abundant lateral microtubule interactions of unattached kinetochores in unperturbed mitosis[4, 22]. 14 Mad2-EGFP dots on unaligned chromosomes localized away from high microtubule density regions, of which 3 Mad2-EGFP dots appeared unattached, whereas 11 Mad2-EGFP dots appeared to interact laterally with faintly stained astral microtubules (Fig. 1d, e). End-on attachments of microtubules to laser-displaced chromosomes, in contrast, were never observed at Mad2-EGFP dots, yet we did detect end-on attachments at chromosome regions opposing single Mad2-EGFP dots (Fig. 1e). Taking the Mad2-EGFP and microtubule localization data together, we conclude that laser microsurgery destabilizes end-on microtubule attachments on displaced chromosomes to induce SAC signaling on one or two sister kinetochores (Fig. 1f).

We next investigated how laser microsurgery affected mitotic progression in HeLa cells (Fig. 2). In the majority of cells (23/35), laser-displaced chromosomes were recaptured by the spindle and recongressed to the metaphase plate during the imaging period of 40 min after cutting. 16/23 cells that had recongressed laser-displaced chromosomes entered anaphase within 40 min after laser microsurgery, yet with significant delay compared to control cells, in which laser microsurgery was performed in regions adjacent to the metaphase spindle (n = 21 cells; Fig. 2a, d; Supplementary Video 1; control cells: 8:59 min:s (median); Fig. 2b, d; Supplementary Video 2; anaphase entry after chromosome displacement and recongression: 30:22 min:s (median); $p = 8.8 * 10^{-6}$ by Mann-Whitney U-test). Thus, SAC-mediated

anaphase delay and recapture by the spindle corrected acute laser-detachment of chromosomes in the majority of cells.

Surprisingly, 11/35 cells entered anaphase in the presence of unaligned chromosomes (Fig. 2c, d; Supplementary Video 3). This is a much higher mitotic slippage rate compared to cells treated with microtubule-depolymerizing drugs: in presence of 100 ng/ml nocodazole, mitotic slippage was never observed within 10 h and it occurred only after 19:09 h:min (median; n = 50 cells). Anaphase entry in presence of unaligned chromosomes occurred with comparable incidence in laser-microsurgery experiments using non-transformed retinal pigmental epithelial cells that have been immortalized by stable overexpression of human telomerase reverse transcriptase (hTERT-RPE1 cells; Supplementary Fig. S2). Thus, a substantial fraction of laser-detached chromosomes bypasses SAC surveillance in cancerous and non-cancerous cells.

What causes the high incidence of mitotic slippage in presence of single unattached chromosomes? One possibility is that the SAC may not re-impose APC/C inhibition fast enough to halt cells once they have progressed to late metaphase stages. Alternatively, single unattached chromosomes may inhibit the APC/C less efficiently than a full complement of unattached chromosomes. This may lead to accelerated mitotic slippage, although it seems unlikely that mitotic slippage can occur within an observation time of less than an hour, given that HeLa cells can arrest for several hours in response to small numbers of unaligned chromosomes[23]. To test these hypotheses, we developed assays to measure the response time and inhibitory strength of the SAC.

To determine how fast a SAC signal is mounted, we measured Mad2 accumulation kinetics in cells stably expressing Mad2-EGFP and H2B-mCherry (Fig. 3a, b; Supplementary Video 4). Mad2-EGFP was first detected on displaced chromosomes 88 ± 39 s (mean ± s.d.; n = 16 cells) after laser microsurgery and reached plateau levels at ~3-4 min (Fig. 3b). Peak levels of Mad2-EGFP on laser-detached chromosomes were similar to those on chromosomes of cells treated with 100 or 500 ng/ml nocodazole (Fig. 3c). Thus, laser-microsurgery leads to fast and efficient recruitment of Mad2 on displaced chromosomes. The relatively high variability observed for Mad2-EGFP recruitment onset could reflect measurement noise owing to the low signal intensities of Mad2-EGFP. It is also possible that mounting a SAC signal on individual kinetochores involves a stochastic process or that Mad2-EGFP accumulation becomes less efficient when cells progress to late stages of metaphase.

We next investigated how fast the APC/C responds to laser microsurgery, by measuring degradation of its fluorescent substrate securin-mEGFP[24, 25], stably expressed in HeLa cells

together with H2B-mCherry[25]. Degradation of EGFP-tagged securin correlates well with that of endogenous securin[24] and stable expression of securin-mEGFP does not perturb mitotic progression[25]. Laser displacement of chromosomes in metaphase cells, which had already started to degrade securin-mEGFP, strongly reduced APC/C activity in 9/11 cells (Fig. 4a, c; Supplementary Fig. S3 and S4; Supplementary Video 5). Significant APC/C inhibition in these cells, however, occurred only after a lag-phase of >5 min (Fig. 4c, e; $p = 1.1 * 10^{-3}$ by t-test with Welch's correction). Two cells entered anaphase shortly after laser microsurgery in presence of unaligned chromosomes and without detectable reduction of securin-mEGFP degradation (Fig. 4b, d; Supplementary Fig. S4; Supplementary Video 6), possibly because they lacked sufficient time to re-impose APC/C inhibition. Previous studies showed that the SAC is inactive during anaphase, when tension is low on kinetochores due to loss of cohesion[26, 27]. Our data indicate that the APC/C becomes unresponsive to chromosome detachment already ~5 min prior to anaphase onset. This marks an irreversible point-of-no-return to exit mitosis and it reveals that SAC inactivation is scheduled before cohesin cleavage, which initiates about 2-3 min prior to anaphase onset[28, 29].

Next, we investigated the extent by which laser-detached chromosomes inhibited the APC/C. At 5-10 min after laser-mediated chromosome displacement, securin-mEGFP was degraded at a rate of 0.60 ± 0.10 %/min (mean ± s.e.m.; n = 9 cells; Fig. 4e). For comparison, we measured the full dynamic range of APC/C activity. Peak activity of APC/C was determined in untreated control cells and in cells depleted of Mad2 by RNAi briefly before the metaphase-anaphase transition (Fig. 5a, c). Securin-mEGFP degraded at a rate of 4.8 ± 0.24 %/min (mean ± s.e.m.) in control cells (n = 10 cells), which was similar to Mad2 RNAi cells (4.8 ± 0.22 %/min; n = 10 cells). Spindle disruption by 100 ng/ml nocodazole strongly inhibited the APC/C to a residual securin-mEGFP degradation rate of 0.085 ± 0.007 %/min (mean ± s.e.m.; n = 10 cells; Fig. 5b, c). Hence, in HeLa cells the SAC has the capacity to impose a ~60-fold inhibition on the APC/C and individual chromosomes inhibited the APC/C significantly less efficiently than complete spindle disruption ($p = 8.3 * 10^{-4}$ by t-test with Welch's correction).

Because APC/C inhibition may not have reached its full extent 5-10 min after chromosome detachment, we aimed to measure APC/C activity for longer time durations. As most laser-displaced chromosomes realigned to the metaphase plate within short time, we searched for an alternative method to induce persistent Mad2 signaling from a small number of kinetochores. We therefore titrated nocodazole to low concentrations (12 - 25 ng/ml) that allowed metaphase plate alignment but induced small numbers of unaligned chromosomes. To test if unaligned chromosomes mounted a SAC signal, we performed immunofluorescence

staining for Mad2 (Fig. 5d, e). In 34 cells with metaphase plates we detected 65 unaligned chromosomes, of which 64 contained bright Mad2 dots, either on one sister kinetochore (Fig. 5d; 27 unaligned chromosomes) or on both sister kinetochores (Fig. 5e; 37 unaligned chromosomes). In contrast, Mad2 did not accumulate on kinetochores of chromosomes aligned on the metaphase plate in 29 cells (5 cells contained one to three weak Mad2 spots on the metaphase plate). Pearson correlation analysis confirms a high correlation between the number of unaligned chromosomes and the number of Mad2-positive kinetochores ($r = 0.81$; $n = 34$ cells).

We next investigated whether APC/C inhibition correlates with the number of unaligned chromosomes (Fig. 5f—h; Supplementary Fig. S5). In presence of a single unaligned chromosome, securin-mEGFP was degraded at 0.32 ± 0.12 %/min (mean ± s.e.m; $n = 15$ cells), which is significantly faster than in cells treated with 100 ng/ml nocodazole (Fig. 5h; $p = 5.6 * 10^{-7}$ by t-test with Welch's correction). In presence of 2-5 unaligned chromosomes, securin-mEGFP was degraded at intermediate rates, whereas in presence of more than 5 unaligned chromosomes degradation rates were similar to those observed in cells treated with 100 ng/ml nocodazole (Fig. 5g, h). These data confirm that a single unattached chromosome can delay anaphase for several hours as previously observed in PtK_1 cells[6]. However, single unaligned chromosomes do not mount a SAC with full inhibitory strength even though they efficiently accumulate Mad2. This results in substantially faster mitotic slippage compared to conditions where all chromosomes are detached from the spindle. Thus, we conclude that the SAC signal is graded and that its inhibitory strength correlates with the number of Mad2-positive kinetochores. This is counter the prevailing view that the SAC functions as a digital switch that is either in an "on" or "off" state.

Aneuploidy and genomic instability are hallmarks of human cancer[30, 31]. Previous studies proposed that merotelic chromosomes, which satisfy the SAC even though they cannot segregate properly, provide a main source of single chromosome aneuploidy[30, 32, 33]. We show that individual unattached or monotelically misattached chromosomes are also prone for missegregation - if they persist for more than 2-3 hours or if they emerge during late metaphase.

The graded response in SAC signaling raises the possibility that an increase in cytoplasmic volume could impair the efficiency of APC/C inhibition per unattached kinetochore. This may be relevant for early divisions of large embryonic cells with weak SAC response[34, 35]. The experimental framework established by our study provides an opportunity to test in future studies whether an increase in cell size can exhaust the SAC signal.

Acknowledgments

The authors thank M. Petronczki and L. Vazquez-Novelle for critical comments on the manuscript, A. Hyman and I. Poser for providing cells expressing Mad2-EGFP, the IMBA/IMP BioOptics core facility and the MBL central microscopy facility for excellent technical support, M. Terasaki and J.M. Peters for helpful discussions and C. Sommer for statistical consultation. Research in the Gerlich laboratory has received funding from the European Community's Seventh Framework Programme FP7/2007-2013 under grant agreements n° 241548 (MitoSys) and n° 258068 (Systems Microscopy), from an ERC Starting Grant (agreement n° 281198), from the EMBO Young Investigator Programme, from the Swiss National Science Foundation, from the Austrian Science Fund (FWF)-funded project "SFB Chromosome Dynamics", and from a Summer Research Award of the Marine Biology Laboratory Woods Hole (Laura and Arthur Colwin Endowed Summer Research Fellowship Fund). A.E.D. is a fellow of the Zurich Ph.D. Program in Molecular Life Sciences and has received funding from a PhD fellowship by the Boehringer Ingelheim Fonds and from a Peter Müller fellowship.

Author contributions

A.E.D. designed and conducted experiments and analyzed data. D.W.G. conceived the project, analyzed data, and wrote the manuscript with help by A.E.D.

Competing financial interests

The authors declare no competing financial interests.

Figure Legends

Figure 1. Laser microsurgery of kinetochore fibers induces Mad2 accumulation on individual displaced chromosomes. (**a**) A live metaphase HeLa cell expressing H2B-mCherry and mEGFP-α-tubulin was imaged by 3D-confocal live-cell microscopy. Kinetochore fiber microtubules were cut with a pulsed 915 nm laser at the area indicated by the white line. The arrowhead indicates a single unaligned chromosome. (**b-e**) Correlative laser microsurgery, time-lapse imaging, and immunofluorescence staining of the spindle. (**b**) A live metaphase HeLa cell expressing H2B-mCherry and Mad2-EGFP was cut with a pulsed 915 nm laser at the area indicated by the white line, and imaged by 3D-confocal live-cell microscopy. (**c**) The cell shown in (b) was fixed 6 min after laser microsurgery and stained for α-tubulin. (**d**) Enlarged region of (c) with linearly increased contrast to enhance visualization of astral microtubules. This reveals lateral microtubule association of a Mad2-positive kinetochore (closed arrowhead), and its sister kinetochore (open arrowhead) localizing to the edge of the spindle. (**e**) Example for unaligned chromosome with single Mad2 accumulation site (solid arrowhead), 2:20 min:s after laser microsurgery (see Supplementary Fig. S1d, e for time-lapse images and overview of cell). The contrast was linearly increased to visualize astral microtubules. Open arrowhead indicates end-on attachment of a microtubule bundle at a chromosome region opposite of the Mad2-positive kinetochore. (**f**) Schematic overview of the laser microsurgery assay. Chromosomes (red), microtubules, kinetochores (gray), and Mad2 (green). Dashed line indicates laser microsurgery. Time = 0:00 min:s at the first image acquired immediately after laser microsurgery. Bars: 10 μm (a-c); 2 μm (d, e).

Figure 2. Fate of cells after laser-induced chromosome detachment. HeLa cells expressing H2B-mCherry and mEGFP-α-tubulin were imaged for 40 min by 3D-confocal live-cell microscopy and cut with a pulsed 915 nm laser at the area indicated by the white lines. Time = 0:00 min:s at the first image acquired immediately after laser microsurgery. (**a**) A representative control cell was cut in a region adjacent to the spindle so that no chromosome was detached. (**b**) A representative cell in which a single chromosome was detached from the mitotic spindle by laser microsurgery. The arrowhead indicates the detached chromosome (2:36), which subsequently recongresses to the metaphase plate (5:49). (**c**) As in (b), but this cell enters anaphase in the presence of an unaligned chromosome

(arrowheads). Bars: 10 μm. (**d**) Fate trajectories of 56 cells cut by laser microsurgery. 21 control cells were cut as in (a), and 35 cells were cut as in (b, c).

Figure 3. SAC response kinetics after laser microsurgery. (**a**) A live metaphase HeLa cell expressing H2B-mCherry and Mad2-EGFP was imaged by 3D-confocal live-cell microscopy and cut with a pulsed 915 nm laser at the area indicated by the white line. Arrowheads indicate site of Mad2-EGFP accumulations on the displaced chromosome. Time = 0:00 min:s at the first image acquired immediately after laser microsurgery. Bar: 10 μm. (**b**) Kinetics of Mad2-EGFP enrichment on detached chromosomes, measured in a circular region with a diameter of 1.2 μm (n = 16 cells). Each curve represents the sister kinetochore with the first Mad2-EGFP accumulation. Red dashed line indicates 3 s.d. above the mean Mad2-EGFP fluorescence on chromosomes before cutting, which served as threshold to detect the onset of Mad2-EGFP accumulation. (**c**) Peak levels of Mad2-EGFP were measured at 4:30 - 5:00 min:s after laser microsurgery, or after spindle depolymerization by nocodazole. Each dot represents one kinetochore.

Figure 4. Kinetics of APC/C inhibition after laser microsurgery. HeLa cells expressing H2B-mCherry and securin-mEGFP were imaged by 3D-confocal microscopy from prophase until metaphase. At different time points during metaphase, the spindle was cut by a pulsed 915 nm laser as indicated by the white line. Time = 0:00 min:s at the first image acquired immediately after laser microsurgery. (**a**) A representative cell in which a detached chromosome (arrowheads) recongressed to the metaphase plate before anaphase entry. (**b**) A cell that enters anaphase in presence of an unaligned chromosome (arrowheads). Bars: 10 μm. (**c, d**) Securin-mEGFP degradation kinetics, normalized to metaphase onset, for the cells shown in (a) or (b), respectively. (**e**) Securin degradation rate was determined by linear interpolation in 11 cells, either before or at different time intervals after laser microsurgery. Error bars indicate mean ± s.e.m.

Figure 5. The inhibitory strength of the SAC correlates with the number of unaligned chromosomes. (**a**) Securin-mEGFP degradation rates peak briefly before anaphase onset. HeLa cells expressing H2B-mCherry and securin-mEGFP were transfected with non-targeting siRNA (control, green curves), or with siRNA targeting Mad2 (blue), and imaged live 24 h after transfection. Total securin-mEGFP fluorescence was measured in individual

cells (n = 10 per condition). Time = 0 min at prometaphase onset. Solid lines indicate pre-anaphase stages; dashed lines indicate post-anaphase stages. (**b**) Securin-mEGFP degradation was measured as in (a) in cells treated with 100 ng/ml nocodazole. (**c**) Securin-mEGFP degradation rates for cells shown in (a, b) were determined by linear regression. Each dot represents one cell. (**d, e**) Low concentrations of nocodazole selectively induce Mad2 accumulation on unaligned chromosomes. Cells treated for 3-5 h with 25 ng/ml nocodazole were fixed and stained with anti-Mad2 and CREST antibodies (n = 34 cells). (d) Cell with a single unaligned chromosome that accumulated Mad2 on a single sister kinetochore. (e) Cell with two unaligned chromosomes, which each accumulated Mad2 on both sister kinetochores. (**f**) A HeLa cell expressing H2B-mCherry and securin-mEGFP was imaged by 3D-confocal microscopy in presence of 12 ng/ml nocodazole. Arrowhead indicates a single unaligned chromosome during anaphase. Time = 0:00 min:s at prometaphase onset. (**g**) Total securin-mEGFP was measured as in (a) for the cell shown in (f). Dashed line indicates post-anaphase stages. See Supplementary Fig. S5 for four more examples and raw measurements. (**h**) Securin-mEGFP degradation was measured in 26 cells treated with 6, 12 or 25 ng/ml nocodazole, using linear regression at different time intervals (each dot represents one measurement that relates to a specific number of unaligned chromosomes, as illustrated in (g)). 13 control cells were treated with 100 ng/ml nocodazole. Error bars indicate mean ± s.e.m. Bars: 10 μm.

References

1. Musacchio, A. & Salmon, E.D. The spindle-assembly checkpoint in space and time. *Nat Rev Mol Cell Biol* **8**, 379-393 (2007).

2. Lara-Gonzalez, P., Westhorpe, F.G. & Taylor, S.S. The spindle assembly checkpoint. *Curr Biol* **22**, R966-980 (2012).

3. Kitajima, T.S., Ohsugi, M. & Ellenberg, J. Complete kinetochore tracking reveals error-prone homologous chromosome biorientation in mammalian oocytes. *Cell* **146**, 568-581 (2011).

4. Magidson, V. *et al.* The spatial arrangement of chromosomes during prometaphase facilitates spindle assembly. *Cell* **146**, 555-567 (2011).

5. Lampson, M.A. & Cheeseman, I.M. Sensing centromere tension: Aurora B and the regulation of kinetochore function. *Trends Cell Biol* **21**, 133-140 (2011).

6. Rieder, C.L., Cole, R.W., Khodjakov, A. & Sluder, G. The checkpoint delaying anaphase in response to chromosome monoorientation is mediated by an inhibitory signal produced by unattached kinetochores. *J Cell Biol* **130**, 941-948 (1995).

7. Brito, D.A. & Rieder, C.L. Mitotic checkpoint slippage in humans occurs via cyclin B destruction in the presence of an active checkpoint. *Curr Biol* **16**, 1194-1200 (2006).

8. Rieder, C.L. & Maiato, H. Stuck in Division or Passing through; What Happens When Cells Cannot Satisfy the Spindle Assembly Checkpoint. *Dev Cell* **7**, 637-651 (2004).

9. Manchado, E. *et al.* Targeting mitotic exit leads to tumor regression in vivo: Modulation by Cdk1, Mastl, and the PP2A/B55alpha,delta phosphatase. *Cancer Cell* **18**, 641-654 (2010).

10. Gascoigne, K.E. & Taylor, S.S. How do anti-mitotic drugs kill cancer cells? *J Cell Sci* **122**, 2579-2585 (2009).

11. Huang, H.C., Shi, J., Orth, J.D. & Mitchison, T.J. Evidence that mitotic exit is a better cancer therapeutic target than spindle assembly. *Cancer Cell* **16**, 347-358 (2009).

12. Yang, Z., Kenny, A.E., Brito, D.A. & Rieder, C.L. Cells satisfy the mitotic checkpoint in Taxol, and do so faster in concentrations that stabilize syntelic attachments. *J Cell Biol* **186**, 675-684 (2009).

13. Reddy, S.K., Rape, M., Margansky, W.A. & Kirschner, M.W. Ubiquitination by the anaphase-promoting complex drives spindle checkpoint inactivation. *Nature* **446**, 921-925 (2007).

14. Nilsson, J., Yekezare, M., Minshull, J. & Pines, J. The APC/C maintains the spindle assembly checkpoint by targeting Cdc20 for destruction. *Nat Cell Biol* **10**, 1411-1420 (2008).

15. Uzunova, K. *et al.* APC15 mediates CDC20 autoubiquitylation by APC/C(MCC) and disassembly of the mitotic checkpoint complex. *Nat Struct Mol Biol* **19**, 1116-1123 (2012).

16. Mansfeld, J., Collin, P., Collins, M.O., Choudhary, J.S. & Pines, J. APC15 drives the turnover of MCC-CDC20 to make the spindle assembly checkpoint responsive to kinetochore attachment. *Nat Cell Biol* **13**, 1234-1243 (2011).

17. Foster, S.A. & Morgan, D.O. The APC/C subunit Mnd2/Apc15 promotes Cdc20 autoubiquitination and spindle assembly checkpoint inactivation. *Mol Cell* **47**, 921-932 (2012).

18. Varetti, G., Guida, C., Santaguida, S., Chiroli, E. & Musacchio, A. Homeostatic control of mitotic arrest. *Mol Cell* **44**, 710-720 (2011).

19. Waters, J.C., Chen, R.H., Murray, A.W. & Salmon, E.D. Localization of Mad2 to kinetochores depends on microtubule attachment, not tension. *J Cell Biol* **141**, 1181-1191 (1998).

20. Lenart, P. *et al.* The small-molecule inhibitor BI 2536 reveals novel insights into mitotic roles of polo-like kinase 1. *Curr Biol* **17**, 304-315 (2007).

21. Liu, D., Davydenko, O. & Lampson, M.A. Polo-like kinase-1 regulates kinetochore-microtubule dynamics and spindle checkpoint silencing. *J Cell Biol* **198**, 491-499 (2012).

22. Kapoor, T.M. *et al.* Chromosomes can congress to the metaphase plate before biorientation. *Science* **311**, 388-391 (2006).

23. Stevens, D., Gassmann, R., Oegema, K. & Desai, A. Uncoordinated loss of chromatid cohesion is a common outcome of extended metaphase arrest. *PLoS One* **6**, e22969 (2011).

24. Hagting, A. *et al.* Human securin proteolysis is controlled by the spindle checkpoint and reveals when the APC/C switches from activation by Cdc20 to Cdh1. *J Cell Biol* **157**, 1125-1137 (2002).

25. Held, M. *et al.* CellCognition: time-resolved phenotype annotation in high-throughput live cell imaging. *Nat Methods* **7**, 747-754 (2010).

26. Vazquez-Novelle, M.D. & Petronczki, M. Relocation of the chromosomal passenger complex prevents mitotic checkpoint engagement at anaphase. *Curr Biol* **20**, 1402-1407 (2010).

27. Mirchenko, L. & Uhlmann, F. Sli15(INCENP) dephosphorylation prevents mitotic checkpoint reengagement due to loss of tension at anaphase onset. *Curr Biol* **20**, 1396-1401 (2010).

28. Gerlich, D., Koch, B., Dupeux, F., Peters, J.M. & Ellenberg, J. Live-cell imaging reveals a stable cohesin-chromatin interaction after but not before DNA replication. *Curr Biol* **16**, 1571-1578 (2006).

29. Shindo, N., Kumada, K. & Hirota, T. Separase sensor reveals dual roles for separase coordinating cohesin cleavage and cdk1 inhibition. *Dev Cell* **23**, 112-123 (2012).

30. Gordon, D.J., Resio, B. & Pellman, D. Causes and consequences of aneuploidy in cancer. *Nat Rev Genet* **13**, 189-203 (2012).

31. Holland, A.J. & Cleveland, D.W. Boveri revisited: chromosomal instability, aneuploidy and tumorigenesis. *Nat Rev Mol Cell Biol* **10**, 478-487 (2009).

32. Cimini, D. *et al.* Merotelic kinetochore orientation is a major mechanism of aneuploidy in mitotic mammalian tissue cells. *J Cell Biol* **153**, 517-527 (2001).

33. Thompson, S.L. & Compton, D.A. Examining the link between chromosomal instability and aneuploidy in human cells. *J Cell Biol* **180**, 665-672 (2008).

34. Glover, D.M. Mitosis in the Drosophila embryo--in and out of control. *Trends Genet* **7**, 125-132 (1991).

35. Sluder, G. Role of spindle microtubules in the control of cell cycle timing. *J Cell Biol* **80**, 674-691 (1979).

Dick and Gerlich, Figure 1

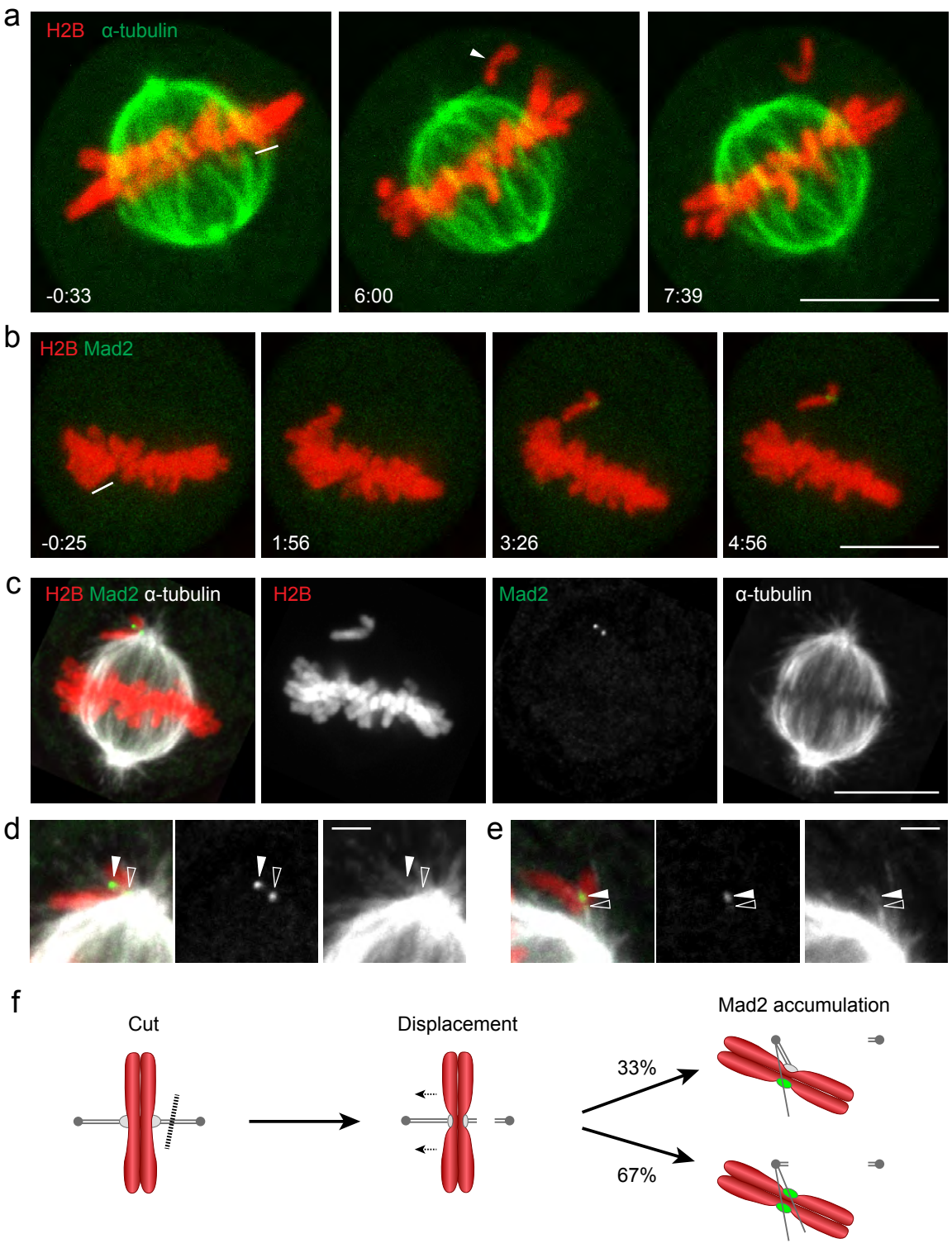

Dick and Gerlich, Figure 2

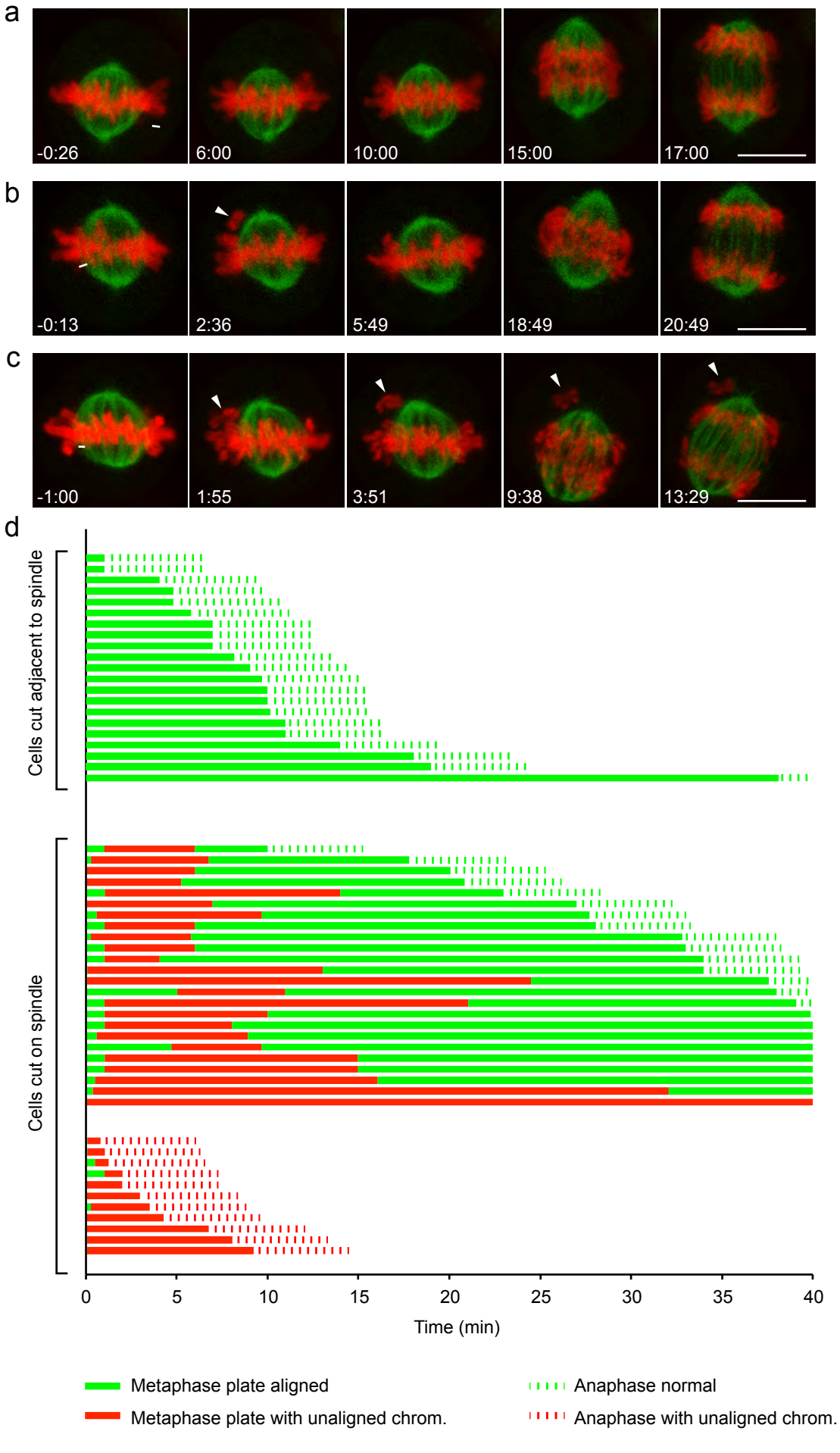

Dick Dick and Gerlich, Figure 3

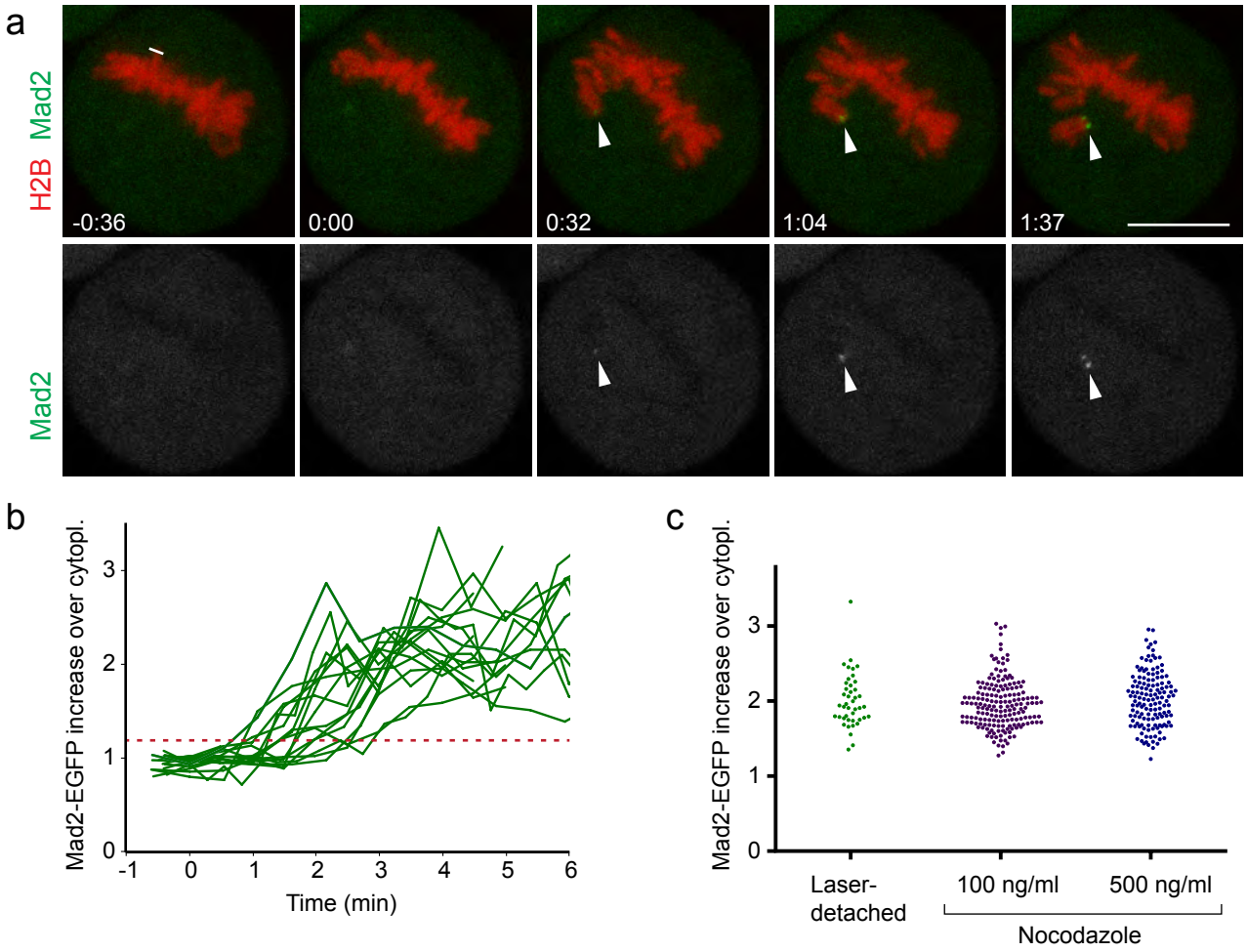

Dick Dick and Gerlich, Figure 4

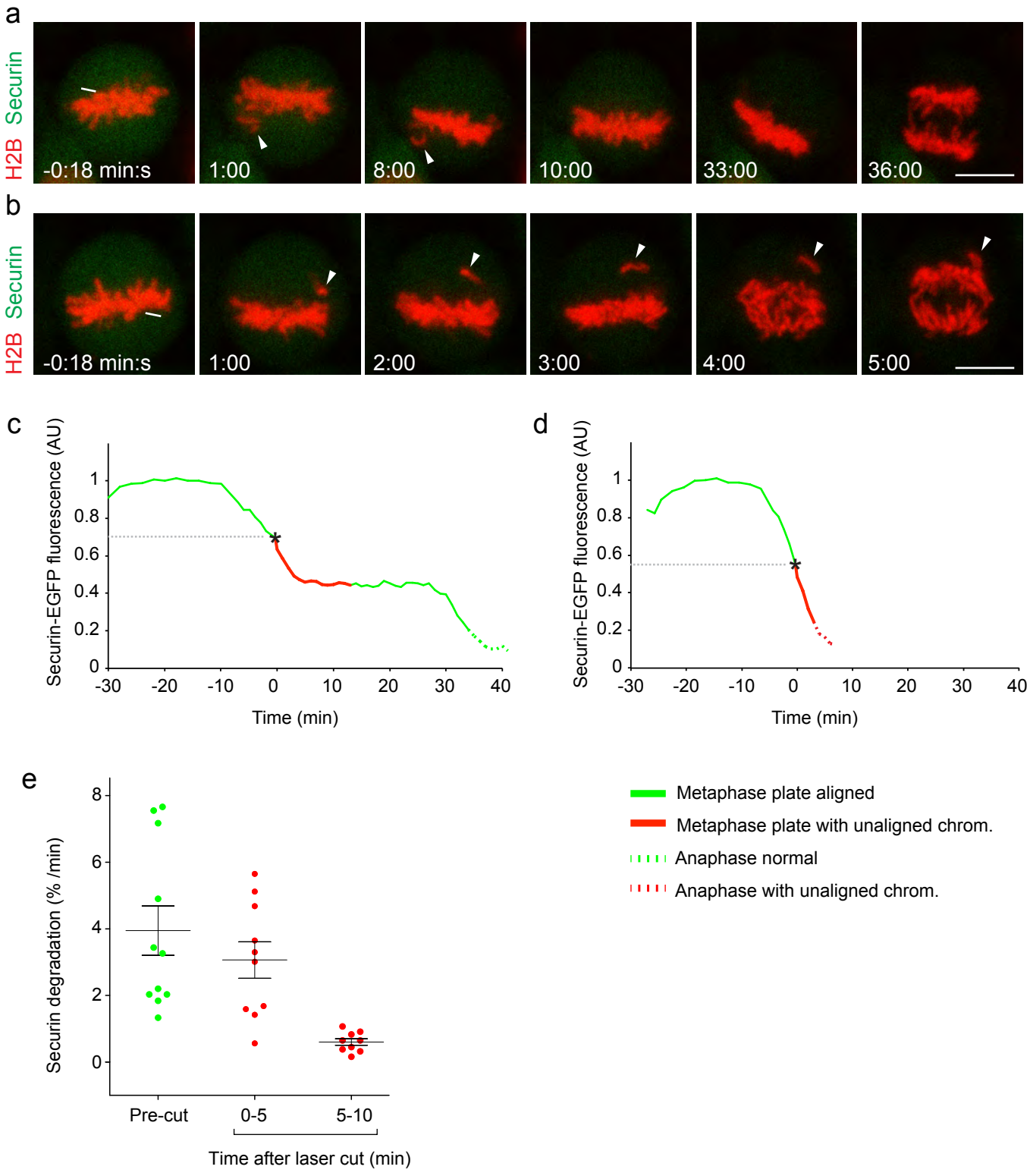

Dick Dick and Gerlich, Figure 5

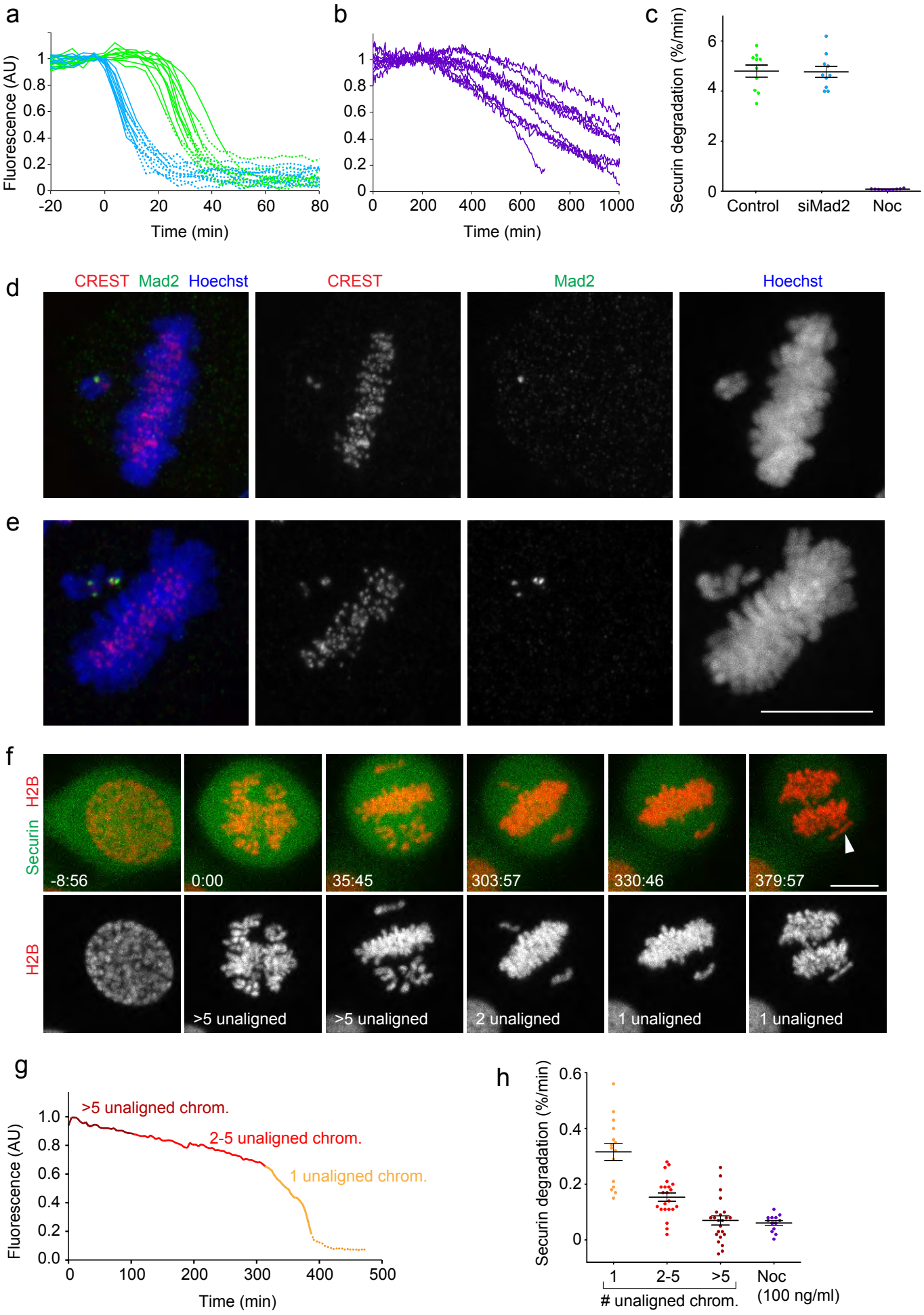

Dick et al., Supplementary Figure S1

a

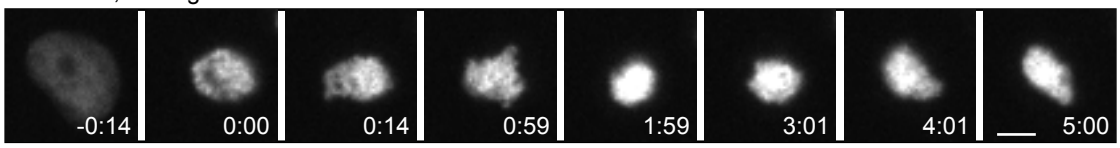

b

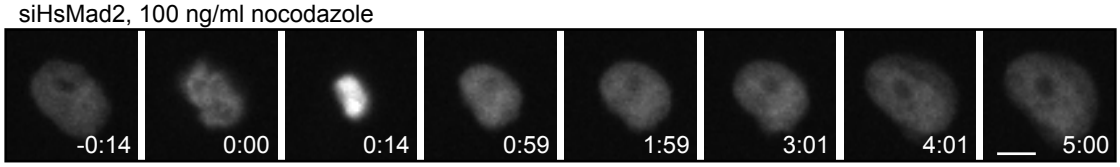

c

Cell line	RNAi: siControl	RNAi: siHsMad2
Securin-EGFP H2B-mCherry	0 %	93 %
EGFP-mmMad2 H2B-mCherry	0 %	0 %

d

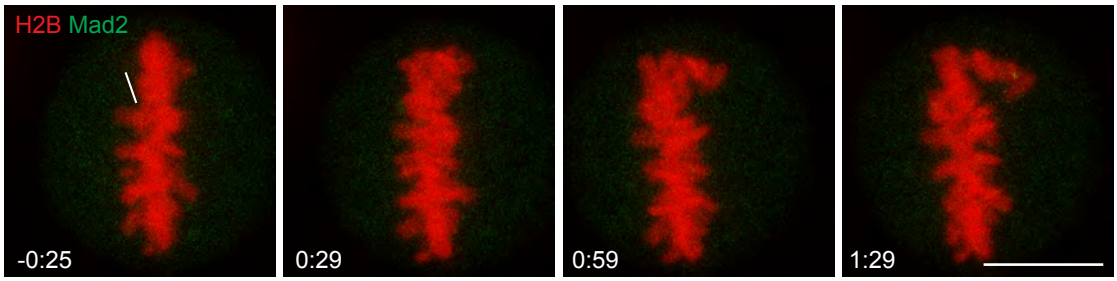

e

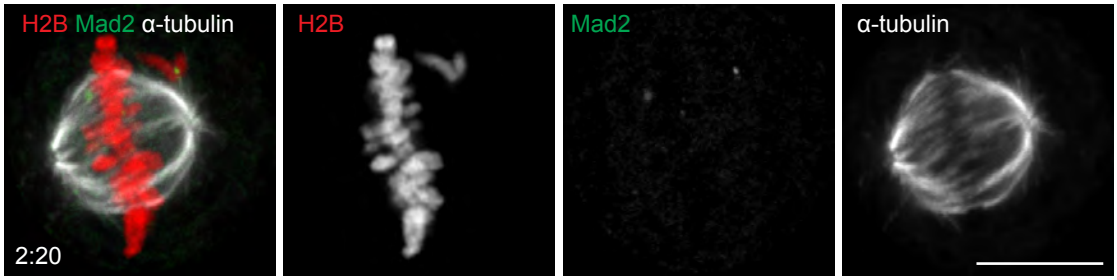

f

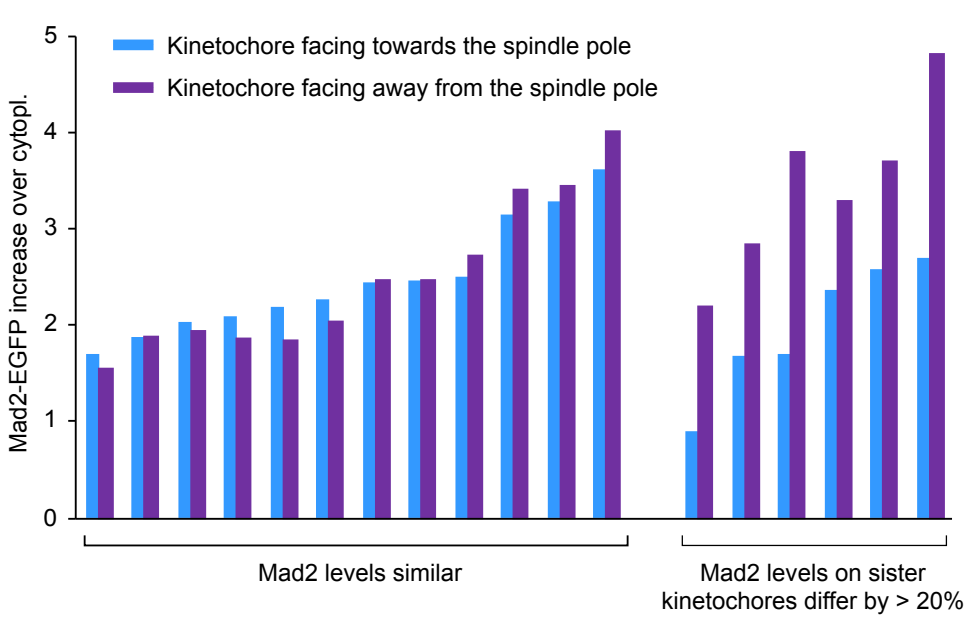

Dick et al., Supplementary Figure 2

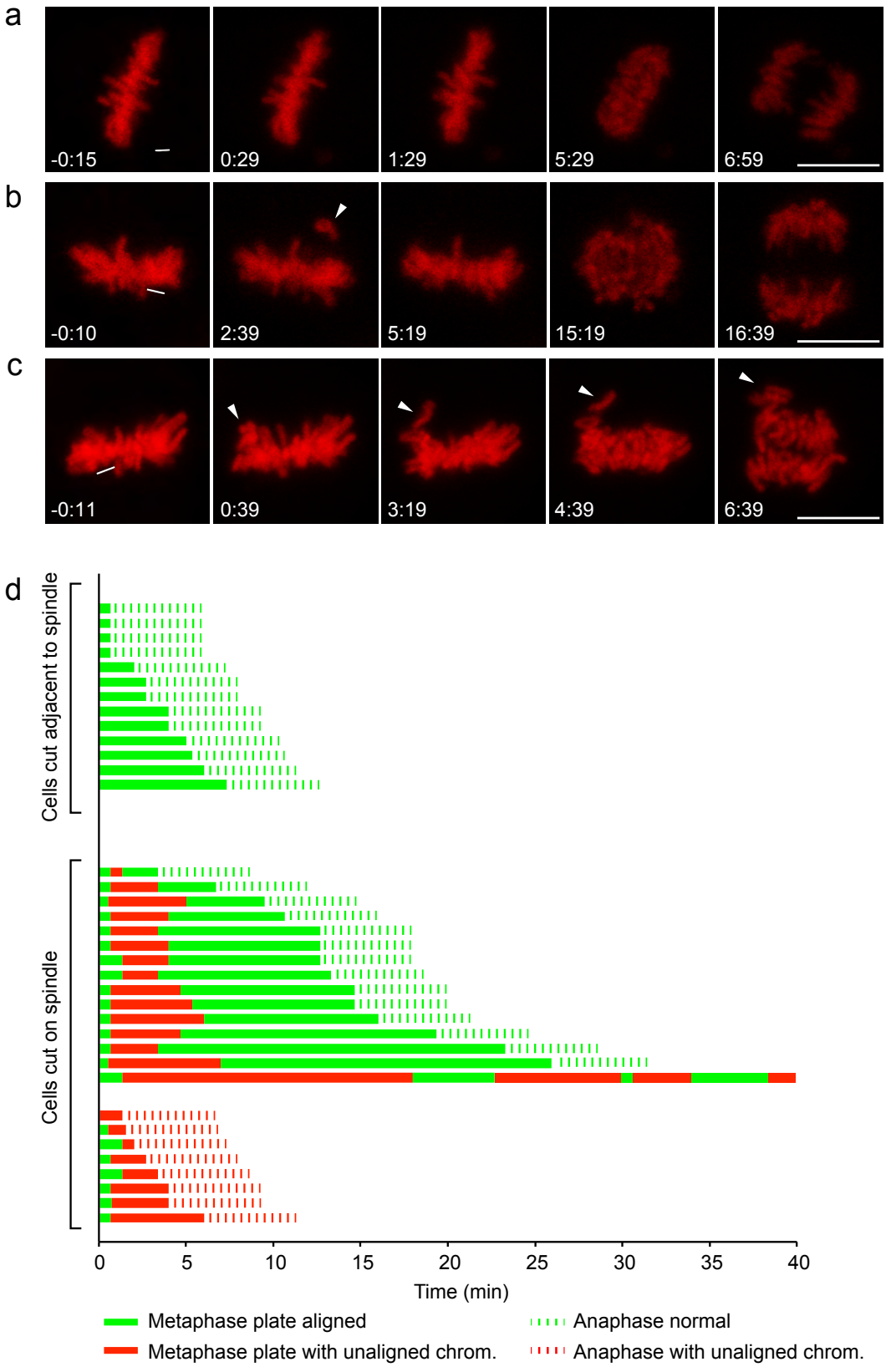

Dick et al., Supplementary Figure S3

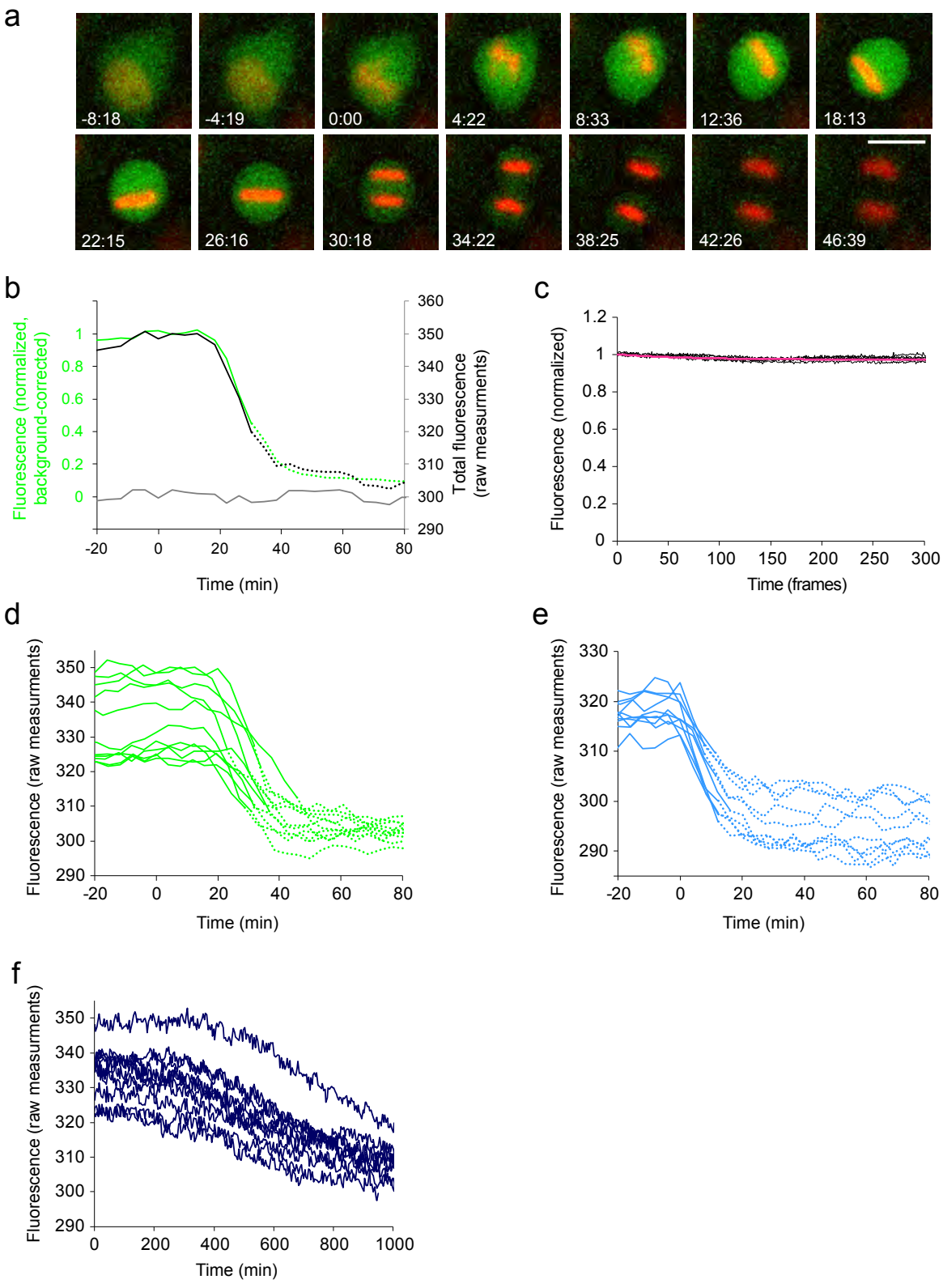

Dick et al., Supplementary Figure S4

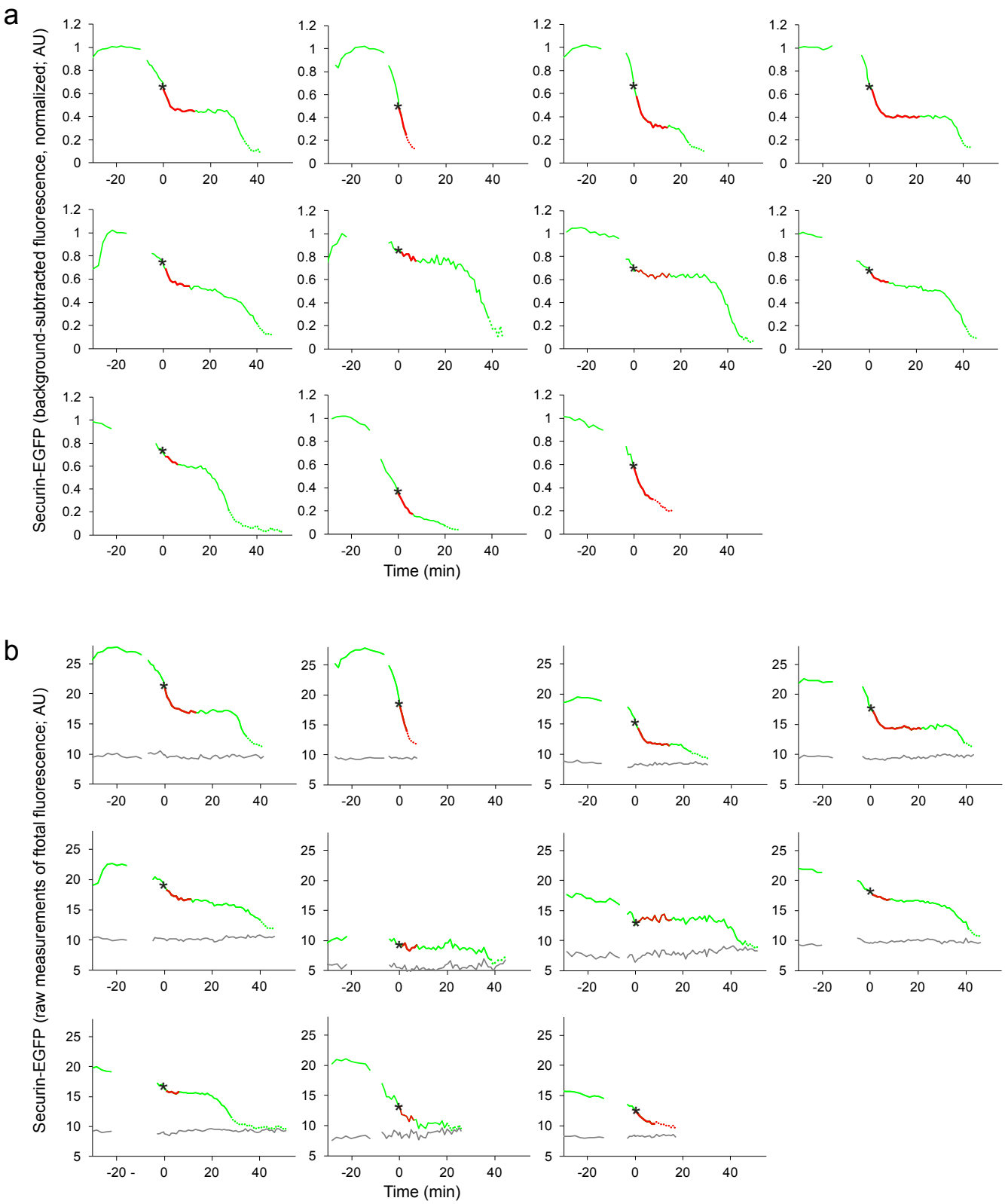

Dick et al., Supplementary Figure S5

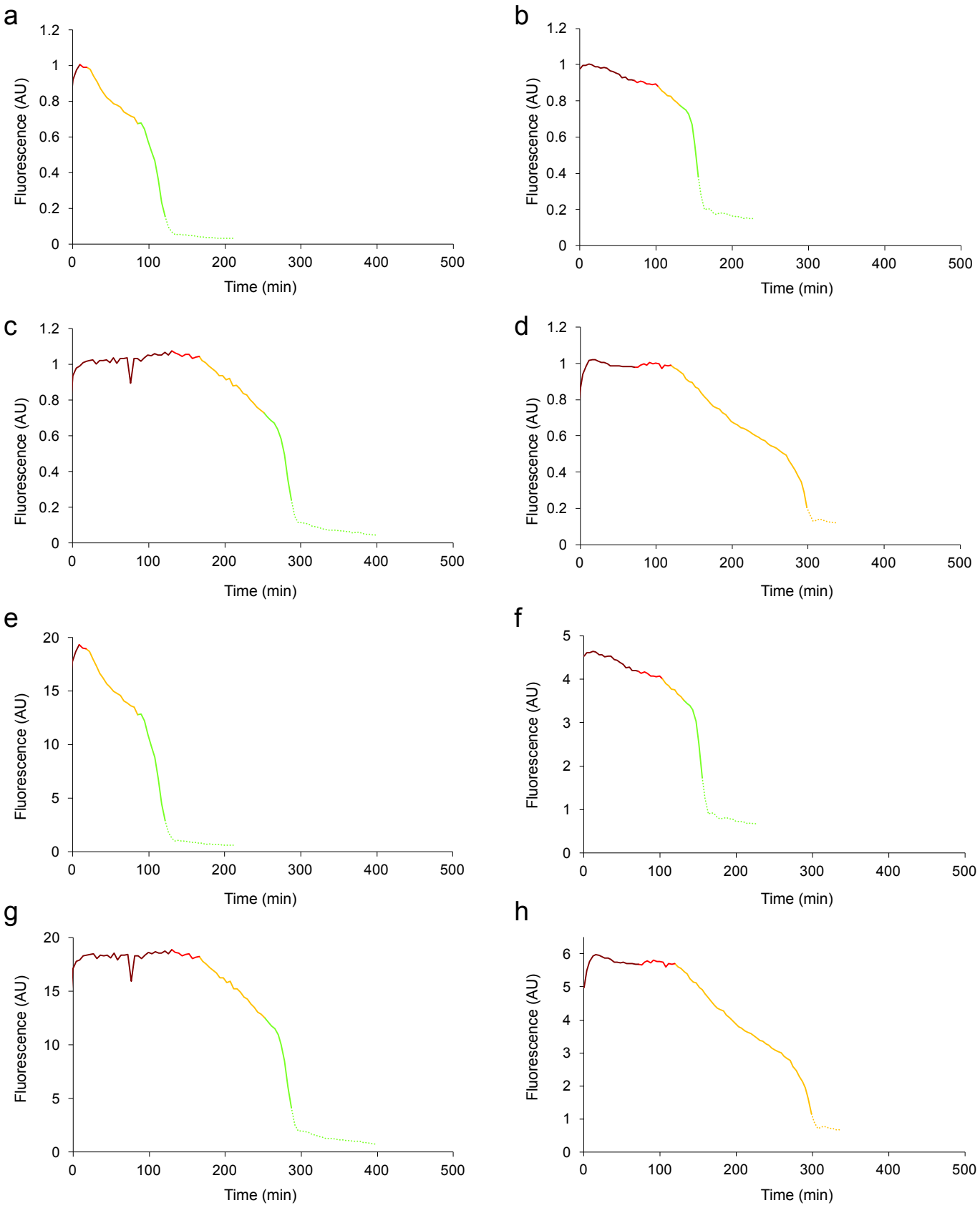

Supplementary Figure Legends

Supplementary Figure S1.

(**a-c)** Validation of the mouse Mad2-EGFP-expressing cell line. (**a**) Prolonged mitosis in presence of 100 ng/ml nocodazole. HeLa cells stably expressing H2B-mCherry and securin-mEGFP were transfected with non-targeting control siRNA and imaged live after 24 h in presence of 100 ng/ml nocodazole. Time = 0:00 h:min at prometaphase onset. (**b**) Mitotic slippage after depletion of Mad2. Imaging was as in (a), but this cell was transfected with siRNA targeting human Mad2 (siHsMad2), 24 h prior to imaging. Bars 5 μm. (**c**) Mitotic slippage induced by transfection of siHsMad2 is suppressed in HeLa cells expressing mouse Mad2-EGFP. Imaging was as in (a, b) using cells stably expressing H2B-mCherry and securin-mEGFP, or H2B-mCherry and mouse-Mad2-EGFP. Mitotic slippage within 3 h after mitotic entry was scored based on the condensation status of H2B-mCherry (n = 30 for each condition). (**d-f**) Correlative laser microsurgery, time-lapse imaging, and immunofluorescence staining of the spindle as in Fig. 1b, c. (d) A live metaphase HeLa cell expressing H2B-mCherry and Mad2-EGFP was cut with a pulsed 915 nm laser at the area indicated by the white line, and imaged by 3D-confocal live-cell microscopy. (e) The cell shown in (d) was fixed 2:20 min:s after laser microsurgery and stained for α-tubulin. Bars: 10 μm. (f) Quantification of Mad2-EGFP levels on both sister kinetochores of 18 laser-displaced chromosomes with two Mad2 positive kinetochores.

Supplementary Figure S2. Fate of non-cancerous retinal pigmental epithelium cells, immortalized by stable overexpression of hTERT (hTERT-RPE1), after laser-induced chromosome detachment. hTERT-RPE1 cells stably expressing H2B-mCherry were cut with a pulsed 915 nm laser at the area indicated with the white lines and imaged by 3D-confocal live-cell microscopy for 40 min. Time = 0:00 min:s at the first image acquired immediately after laser microsurgery. (**a**) A representative control cell was cut in a cytoplasmic region away from the spindle so that no chromosome was detached. (**b**) A representative cell in which a single chromosome was displaced from the metaphase plate by laser microsurgery, which subsequently recongresses before anaphase onset. (**c**) As in (b), but this cell enters anaphase in presence of an unaligned chromosome. Bars: 10 μm. (**d**) Fate trajectories of 36 cells, of which 13 control cells were cut adjacent to the spindle without perturbing the metaphase plate, and 23 cells were cut on the spindle to displace one or few chromosomes from the metaphase plate.

Supplementary Figure S3. Analysis of securin-mEGFP degradation. (a) Original image frames of a HeLa cell stably expressing securin-mEGFP and H2B-mCherry. (b) Raw

measurements of total mEGFP-securin fluorescence (black curve; scale is indicated to the right of the plot), overlaid on background-subtracted and bleach-corrected curve normalized to prometaphase (green, scale on left y-axis). Solid line indicates pre-anaphase stages, dashed line indicates post-anaphase stages. Light gray line indicates background, measured in a region adjacent to the cell. (c) Acquisition photobleaching was measured in a mitotic cell treated with 200 ng/ml nocodazole, with fast time-lapse to minimize the effect of mitotic slippage degradation (time-lapse: 2.7 s/frame). An exponential function (pink curve) was fitted to 5 bleach measurements (black curves). This function was determined separately for each experimental condition to correct for acquisition photobleaching as indicated in the online methods. (d) Raw total fluorescence measurements for the data shown in Fig. 5a (control cells, non-targeting siRNA). (e) Raw total fluorescence measurements for the data shown in Fig. 5a (Mad2 RNAi). (f) Raw measurements for the data shown in Fig. 5b.

Supplementary Figure S4. Kinetics of APC/C inhibition after chromosome detachment for 11 cells, as shown for two selected examples in Figure 4c, d. HeLa cells expressing H2B-mCherry and securin-mEGFP were imaged by 3D-confocal microscopy from prophase until metaphase. At different time points during metaphase (indicated by black star), the spindle was cut by a pulsed 915 nm laser to detach individual chromosomes. Time = 0 min at the first image acquired immediately after laser microsurgery. Red indicates time points where individual chromosomes were dealigned from the metaphase plate. Dashed lines indicate anaphase, with (red) or without (green) unaligned chromosomes. The gaps in the curve indicate pauses during time-lapse imaging to reduce light exposure. (a) Background-subtracted total fluorescence was normalized to prometaphase as shown in Fig. 4c, d. The first two panels represent the cells shown in Fig. 4. (b) Raw measurements of total fluorescence intensity in mean intensity projections of z-stacks. Gray curves indicate measurements outside cells used for background subtraction.

Supplementary Figure S5. Four additional examples for securin-mEGFP degradation in correlation with unaligned chromosomes induced by low dose nocodazole. HeLa cells expressing H2B-mCherry and securin-mEGFP were imaged and analyzed as in Fig. 5f, g. Dark red indicates time intervals with >5 unaligned chromosomes, light red indicates time intervals with 2-5 unaligned chromosomes, orange indicates one unaligned chromosome, green indicates alignment of all chromosomes. Solid lines indicate pre-anaphase stages, dashed lines indicate anaphase stages. (a-d) Background-subtracted and bleach corrected total fluorescence normalized to prometaphase. (a) Cell treated with 6 ng/ml nocodazole. (b) 25 ng/ml nocodazole. (c, d) 12 ng/ml nocodazole. (e-h) Background-subtracted raw measurements of the cells shown in a-d.

Online Methods

Cell culture

Stably expressing cell lines were derived from the HeLa 'Kyoto' cell line obtained from S. Narumiya (Kyoto University, Japan) or from hTERT-RPE1 obtained from P. Meraldi (University of Geneva, Switzerland). Monoclonal reporter cell lines were generated as previously described[36] and cultured in Dulbecco's modified eagle medium (DMEM; GIBCO) supplemented with 10% (v/v) fetal bovine serum (FBS) (PAA Laboratories), 1% (v/v) penicillin–streptomycin (Invitrogen), 500 µg/ml G418 and 0,5 µg/ml puromycin. For live-cell microscopy, cells were grown either in 96-well plastic-bottom plates (µclear; Greiner Bio-One Ltd.), or on LabTek II chambered coverslips (ThermoScientific). Live cell imaging was performed in DMEM containing 10% (v/v) FBS and 1% (v/v) penicillin/streptomycin, but without phenolred and riboflavin to reduce autofluorescence of the medium[36]. Laser microsurgery experiments were performed in Leibovitz L-15 medium (GIBCO) containing 10% FBS.

RNAi and drug treatment

Cells were transfected ~ 24 h before imaging in 96-well plastic-bottom plates (µclear; Greiner Bio-One Ltd.) with HiPerfect (Qiagen) or Lipofectamine RNAiMax (Invitrogen) according to the manufacturer's instructions. Mad2 siRNA targeting sequences: 5'-AAGAGTCGGGACCACAGTTTA-3' (Qiagen) (Supplementary Fig. 1) and 5'-TTACTCGAGTGCAGAAATA-3' (Dharmacon) (Fig. 5). The non-targeting control siRNA was AllStars (Qiagen). Final siRNA concentration was 10 nM. Nocodazole (Sigma) was dissolved to final concentrations of 100 ng/ml to disrupt the entire spindle, or 6-25 ng/ml to induce metaphase plates with persistent unaligned chromosomes (Fig. 5d-f).

Indirect immunofluorescence staining

For correlative microtubule immunofluorescence staining after laser microsurgery (Fig. 1b-e) 16% (w/v) formaldehyde solution (methanol-free, ThermoScientific) was added directly to the medium to a final concentration of 4%. Cells were fixed for 7:30 min:s and then washed with PBS/0.05% Tween20. This was followed by 5 min permeabilization with PBS/0.5% Triton X-100. Cells were blocked for 10 min with 10% FCS in PBS / 0.05% Tween20 and stained for 1 h with mouse monoclonal anti-α-tubulin antibody (1:1,000; clone DM1A, mouse

ascites fluid; Sigma T9026, lot #: 052M4837). Cells were then stained for 30 min with goat anti-mouse IgG Alexa Fluor 633 (1:600; Molecular Probes).

To stain Mad2 after low-dose nocodazole treatment (Fig. 5d, e), cells were fixed and simultaneously extracted with 4% formaldehyde diluted in PTEM buffer (20 mM PIPES, pH 6.8, 0.2%Triton X-100, 10 mM EGTA, 1mM $MgCl_2$) for 7 min. Cells were blocked for 30 min with 3% BSA in PBS before staining for 1 h with rabbit polyclonal anti-Mad2 (1:1,000; Bethyl, lot #: 300-301 A-1) and human anti-centromere antibodies (CREST) (1:400; Antibodies Incorperated). Subsequently cells were stained for 30 min with donkey anti-rabbit IgG Alexa Fluor 488 and goat anti-human IgG Alexa Fluor 594 (1:600; Molecular Probes, respectively). DNA was stained with 2 µg/ml Hoechst 33342 (Sigma).

Microscopy and laser microsurgery

Automated wide-field fluorescence microscopy was performed on a Molecular Devices ImageXpressMicro XL screening microscope equipped with reflection-based laser autofocus and a 10x 0.5 N.A. S Fluor dry objective (Nikon), controlled by in-house developed Metamorph macros[21]. Cells were maintained in a microscope stage incubator at 37ºC in humidified atmosphere of 5% CO_2 throughout the entire experiment. Illumination was adjusted that cell death rate was below 5% in untreated control cells.

Confocal microscopy was performed on a customized Zeiss LSM780 microscope using a 40x 1.4 N.A. Oil DIC Plan-Apochromat objective (Zeiss), controlled by ZEN 2011 software and an autofocus macro (AutofocusScreen) kindly provided by J. Ellenberg. The microscope was equipped with an EMBL incubation chamber (European Molecular Biology Laboratory), providing a humidified atmosphere at 37°C with 5% CO_2.

Laser microsurgery was performed on a Zeiss LSM710 confocal microscope equipped with a tuneable Chameleon Ti:Sapphire laser for multi-photon excitation using a 63x 1.4 N.A Oil DIC Plan-Apochromat objective (Zeiss), controlled by a ZEN 2010 software. A 37°C atmosphere was provided by a stage incubator and an objective heater. Single chromosome detachment was achieved by tuning the Ti:Sapphire laser to 915 nm and 100% power, and scanning with slow speed in a highly elongated polygon resembling a single line, placed at the edge of the mitotic spindle.

Image analysis

Microscopy images were processed and analyzed using Fiji[37]. 3D-confocal time-lapse images contained 5-10 z-sections. 3D-confocal microscopy of immunofluorescence samples contained 7-30 z-sections (Fig.1c-f), and sampled the entire metaphase plate and all unaligned chromosomes in the experiment shown in Fig. 5d, e. To display fine image structures, maximum intensity projection was applied to selected z-sections that contained the relevant structures (e.g., laser-displaced chromosomes), or the entire cell. Figures or Videos display single z-sections (Fig. 1a), or projections of 2 z-sections (Fig. 3a, 4a, b; Supplementary Video 4-6), 3 z-sections (Fig. 1b-e, 2a-c, Supplementary Fig. S2a-c Supplementary Fig. S1d, e, Supplementary Video S1-3), 9 z-sections (Fig. 5f, Supplementary Video 7)), or 30 z-sections (Fig. 5d, e). To preserve quantitative information of securin-mEGFP also in the displayed image frames, full stacks were projected by mean intensity (Fig. 4a, b and 5f, Supplementary Video 5-7).

Cell fate analysis after laser-induced chromosome detachment (Fig. 2d) was performed with cells expressing H2B-mCherry and mEGFP-α-tubulin, or H2B-mCherry and securin-mEGFP.

To measure Mad2-EGFP levels on sister kinetochores after laser induced chromosome displacement and subsequent fixation (Fig. 1d-f, Supplementary Fig. S1e, f), Mad2 intensity was measured in individual z-sections on chromosomes containing two Mad2 spots, within a circular region with 0.91 μm diameter for each sister kinetochore. To calculate Mad2-EGFP increase over cytoplasm the cytoplasmic EGFP background and image background were measured in the corresponding z-section. Mad2 peak levels (Fig. 3c) and recruitment kinetics (Fig. 3b) were measured on displaced chromosomes that remained unaligned for at least 5 min in cells, and only in cells that did not enter anaphase within 3 min after cutting. Mad2 accumulation was measured on individual displaced chromosomes that could be followed throughout the time series. Mad2-EGFP fluorescence was measured in single z-sections in a circular region of interest with 1.2 μm diameter. Prior to laser microsurgery, EGFP fluorescence was measured in the central z-slice at the chromatin/cytoplasm interface near the cut. Following laser microsurgery, the Mad2-EGFP spot appearing on the first sister kinetochore was followed over time in the z-slice with the highest EGFP signal on the respective chromosome. Cytoplasmic EGFP and image background were measured as described before. The onset of Mad2 recruitment was determined based on an increase of Mad2-EGFP above a threshold of 3 s.d. above the mean Mad2-EGFP fluorescence before the cut. Exact timing for onset of Mad2 recruitment was derived by intersection of the detection threshold and a linear interpolation between Mad2-EGFP measurements. Mad2-EGFP intensities were also measured in cells entering mitosis in presence of 100 or 500 ng/ml nocodazole (Fig. 3c) about 3 min after NEBD. All spots visible within the middle z-section

were quantified in 3D movies, using imaging settings and analysis procedures identical to those in laser microsurgery experiments.

Securin-mEGFP fluorescence after laser microsurgery (Fig. 4c, d) was measured in mean intensity projections of confocal 3D time-lapse images. First, the rate of photobleaching was measured in a fast time-lapse recording of a cell treated with 100 or 200 ng/ml nocodazole. A single exponential function was fitted to the mean fluorescence, serving as a reference function to compensate for acquisition photo-bleaching (Supplementary Fig. S3c). Securin-mEGFP levels were normalized to prometaphase. Rates of securin-mEGFP degradation prior to cutting were determined by linear regression of preceding data points of at least 3 min (Fig. 4e).

To determine the dynamic range of APC/C activity (Fig. 5a-c), total securin-mEGFP intensity was measured in wide field time-lapse images and bleach corrected as described above. Control and Mad2 RNAi data were normalized to 8-0 min before prometaphase. Cells treated with 100 ng/ml nocodazole were normalized to 0-300 min after prometaphase onset to compensate for cell rounding artifacts. Rates of securin-mEGFP degradation were determined by linear regression of data points 12-0 min before anaphase onset (control and Mad2 RNAi), or 20 min after prometaphase onset until mitotic exit (100 ng/ml nocodazole). A small fraction of cells that died in mitosis was omitted from the measurement of mitotic slippage timing.

In the experiments shown in Fig. 5f-h, the number of unaligned chromosomes was determined by visual inspection of confocal 3D image stacks. Securin-mEGFP fluorescence in these movies was measured in mean intensity projections, normalized to 8-12 min after prometaphase onset. Securin-mEGFP degradation rates were calculated by linear regression at time frames in which either 1, 2-5, or >5 unaligned chromosomes persisted longer than 22 min.

Statistical analysis

All data in this manuscript were tested for normality (D'Agostino-Pearson omnibus test (α = 0.05; using the software GraphPad Prism) and for equal variances (Levene's test (α = 0.05; using the software R). Data with normal distribution were presented as mean ± s.d. or mean ± s.e.m, whereas data that had no normal distribution were presented as median values. The appropriate statistical test was chosen accordingly: Normal distributed data with different variances were tested with a two-tailed unpaired t-test with Welch's correction (Fig. 4e; comparison of "5-10 min" in Fig. 4e with "Noc" in Fig 5c; Fig. 5h). Data with non-normal distribution, but equal variances were tested with a two-tailed Mann-Whitney U test (Fig.2d). Statistical significance was determined at α = 0.01 using the software R.

Experimental replicates and sample numbers were as follows: laser microsurgery with correlative immunofluorescence staining of microtubules (Fig. 2b-e) was performed in 18 laser microsurgery experiments (18 cells in 18 different wells) on 3 different days. Mitotic cell fate of HeLa cells after laser microsurgery (Fig. 2) was investigated in 56 experiments (35 cells with displaced chromosomes; 21 control cells cut in cytoplasm adjacent to spindle), which were recorded on 17 different days. Mitotic slippage timing in presence of 100 ng/ml was determined in 3 independent experiments. Kinetics of Mad2 accumulation to displaced chromosomes (Fig. 3b) was measured in 16 cells in 16 independent laser microsurgery experiments performed on 6 different days. For Fig. 3c, Mad2 levels were measured in 20 cells (each in an independent laser microsurgery experiment) recorded on 6 different days, and 11 cells treated with 100 or 500 ng/ml nocodazole were derived from 3 independent experiments, respectively. Securin degradation kinetics after acute chromosome displacement (Fig. 4, Supplementary Fig. S4) were quantified in 11 cells (each in an independent laser microsurgery experiment), on 6 different days. For the dynamic range measurement of the SAC (Fig. 5a-c; Supplementary Fig. S3) securin degradation kinetics were recorded in 3 independent experiments and quantified in 10 cells per condition. Mad2 immunofluorescence staining (Fig. 5d,e) was performed in 34 cells treated with low dose nocodazole in 3 independent experiments. Quantification of securin degradation kinetics after drug-induced spindle disruption (Fig. 5f-h; Supplementary Fig. S5) was performed in 13 cells treated with 100 ng/ml nocodazole, and 26 cells treated with low-dose nocodazole (6-25ng/ml) were imaged in 3 independent experiments. Functionality of mouse Mad2-EGFP was determined in 3 independent experiments by quantification of mitotic timing in 30 cells per condition. The fate of hTERT-RPE1 cells after laser microsurgery (Supplementary Fig. S2) was investigated in 35 cells (each in an independent laser microsurgery experiment) performed on 7 different days.

References

36. Schmitz, M.H. & Gerlich, D.W. Automated live microscopy to study mitotic gene function in fluorescent reporter cell lines. *Methods Mol Biol* **545**, 113-134 (2009).

37. Schindelin, J. *et al.* Fiji: an open-source platform for biological-image analysis. *Nat Methods* **9**, 676-682 (2012).